Cell Reports, Volume *23*

Supplemental Information

Involvement of Mossy Cells in Sharp Wave-Ripple Activity *In Vitro*

Aarti Swaminathan, Ines Wichert, Dietmar Schmitz, and Nikolaus Maier

Inventory of Supplemental Information

The Supplemental Information contains the following items:

Supplemental Figures S1 – S4; these figures add information related to the respective figures shown in the main part of the manuscript

Supplemental Experimental Procedures – a section detailing experimental methods

A

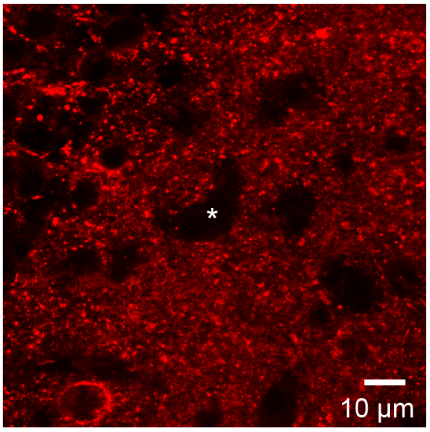

B

Intrinsic physiological properties of mossy cells	
Resting membrane potential (mV)*	-60.1 ± 1.4
Input resistance (MΩ)	312.8 ± 30.7
Action potential	
Threshold (mV)	-40.0 ± 0.8
Amplitude (mV)	70.5 ± 2.8
Duration at 50% of AP maximum (ms)	0.9 ± 0.03
Afterhyperpolarization amplitude (mV)	6.5 ± 0.8
Sag potential amplitude (mV)	7.0 ± 0.8

*no LJP correction; Values are expressed as mean ± S.E.M.; *n* = 12 MCs *N* = 7 mice
95% CIs: RMP: [-63.1 mV -57.1 mV]; Ri: [245.3 MΩ 380.4 MΩ]; AHP: [4.7 mV 8.3 mV]

C

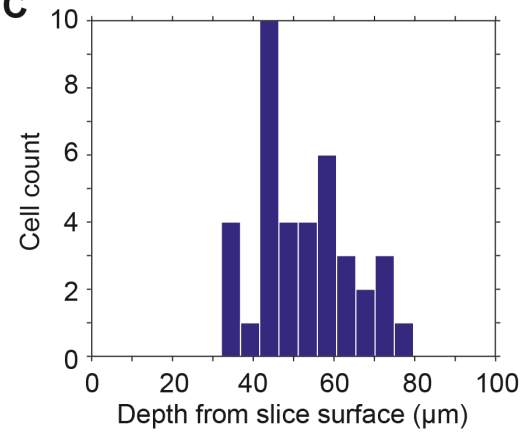

D

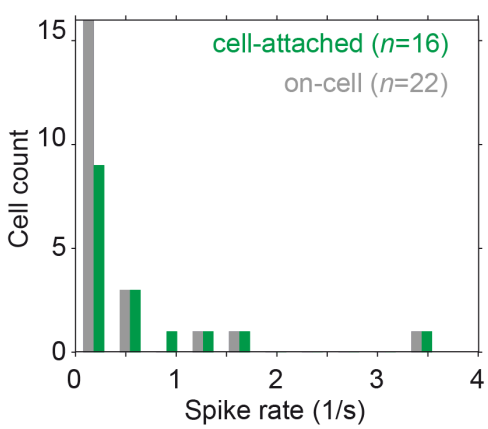

Figure S1. Additional analyses of mossy cell properties. Related to Figure 1.

A GAD67 staining demonstrates the absence of this inhibitory marker on MCs in our sample. The *asterisk* marks the cell displayed in the main Figure 1A. **B** Intrinsic physiological properties of the recorded MCs (n = 12). *Initial resting membrane potential* (RMP) was determined in current-clamp immediately after rupturing the cell membrane. *Input resistance* (R_i) was calculated based on -4 mV steps (50 ms duration) in voltage-clamp, repeated 100 times to minimize the influence of spontaneous synaptic inputs. Trace segments of 10 ms duration with minimal SDs for baseline and steady-state were chosen, averaged, and their means subtracted (ΔI). The voltage step size (-4 mV) was then divided by ΔI to calculate the cell's R_i. *Action potential* (AP) parameters were determined from spikes recorded at rheobase. *AP threshold*, V_{thres}: the membrane potential where dV/dt of the rising phase exceeded 20 mV/ms; *peak amplitude* of APs: measured from V_{thres} to the peak; *width* of APs: the time difference between the points where the rising- and the decaying phases of the AP crossed 50% of its peak amplitude; *afterhyperpolarization* amplitude: the voltage difference between V_{thres} and the most negative deflection immediately following the peak of the AP; *sag potential* amplitude: the voltage difference between the minimum voltage in response to the current injection (-120 pA, 1 s) from the RMP and the steady-state response. **C** Histogram showing the depth distribution of the recorded cells from the surface of the slice (range: 32 to 80 µm). **D** Comparison of the *overall* spike rates, *i.e.*, the total number of spikes divided by the recording time of the individual experiment (on-cell recordings: mean: 0.44 ± 0.12/s; median: 0.08/s, n = 22 cells, N = 11 mice; cell-attached recordings: mean: 0.66 ± 0.22/s; median: 0.3/s, n = 16 cells, N = 9 mice; not different, P = 0.067, two-tailed Mann-Whitney U test).

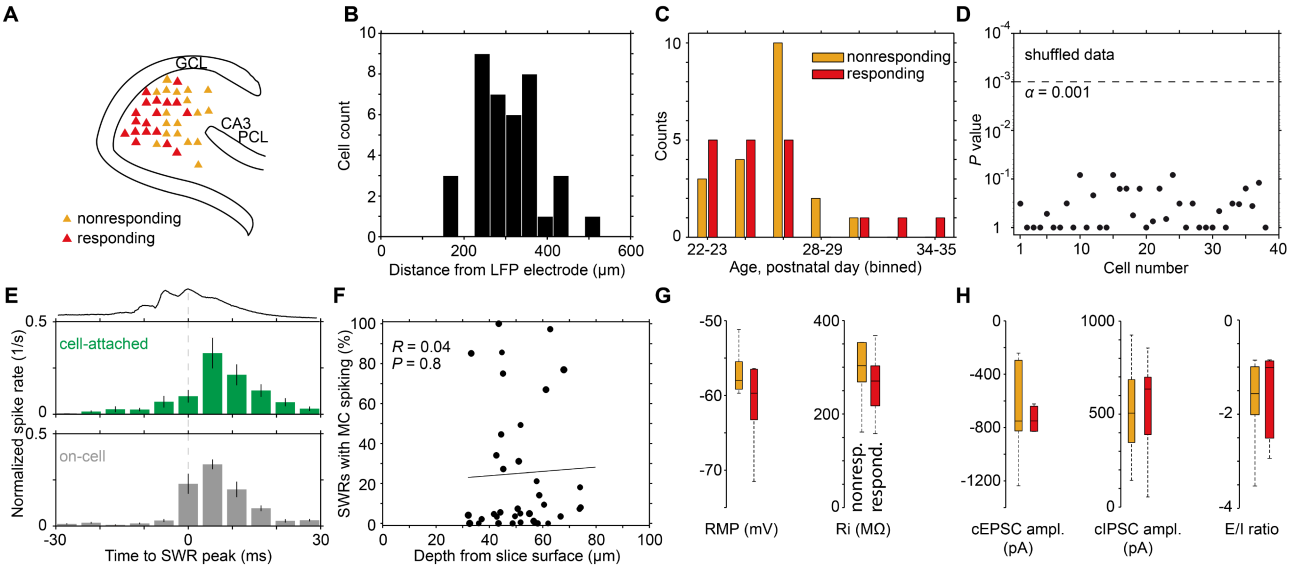

Figure S2. Analysis of SWR-related spiking in MCs in vitro. Related to Figure 2.

A Sketch of the recording location within the hilus of analyzed MCs. *Abbreviations:* GCL, granule cell layer; PCL, pyramidal cell layer. **B** Histogram summarizing the distribution of distances between the LFP electrode in CA3c and the recorded MCs (range: 149 to 529 µm). For all cell-attached recordings, data of at least 6 min after GΩ seal formation were discarded to ensure stabilization of the LFP. **C** Histogram of responding and nonresponding MCs within the range of ages tested (P 22-35; each bin represents the sum of observations in two days). **D** Control related to the analysis shown in the main Figure 2B. Comparison of spiking in shuffled data: In each cell, two spike distributions *N1* and *N2* of *n* randomly sampled periods from the entire trace (where *n* matched the number of detected SWRs in the respective experiment) were compared (Mann-Whitney *U* test). The distribution of *P* values lies clearly above the chosen significance threshold α = 0.001, demonstrating the robustness of SWR-related spiking in MCs (see main Figure 2B) against data shuffling. Values are plotted according to the order of recordings (*x*-axis, as in the main Figure 2B-C). **E** Plots related to the histogram shown in the main Figure 2F to demonstrate the spike-time distribution with reference to the SWR peak (LFP average, *top*); however, here, data were separated according to the recording technique applied (*green:* cell-attached, and *grey:* on-cell). **F** No correlation between SWR-related spiking and depth of the recordings was found. **G and H** Comparisons of different intrinsic and synaptic parameters in responding (resp.) and nonresponding (nonresp.) cells; an unpaired nonparametric test (Mann Whitney *U* test) was applied in all cases. **G** *Left*: Resting membrane potential (RMP, P = 0.25, n = 10 and n = 11 for responding and nonresponding cells). *Right:* Input resistance (R_i, P = 0.32, n = 10 and n = 10 for responding and nonresponding cells). **H** *Left*: SWR-associated cEPSC amplitudes (P = 0.67, n = 7 and n = 11 for responding and nonresponding cells); *Middle:* SWR-associated cIPSC amplitudes (P = 0.81, n = 7 and n = 11 for responding and nonresponding cells); *Right*: For each cell, charge transfer values of excitatory and inhibitory SWR-associated PSCs were determined and their ratios plotted (E/I ratio, P = 0.54, n = 7 and n = 11 for responding and nonresponding cells).

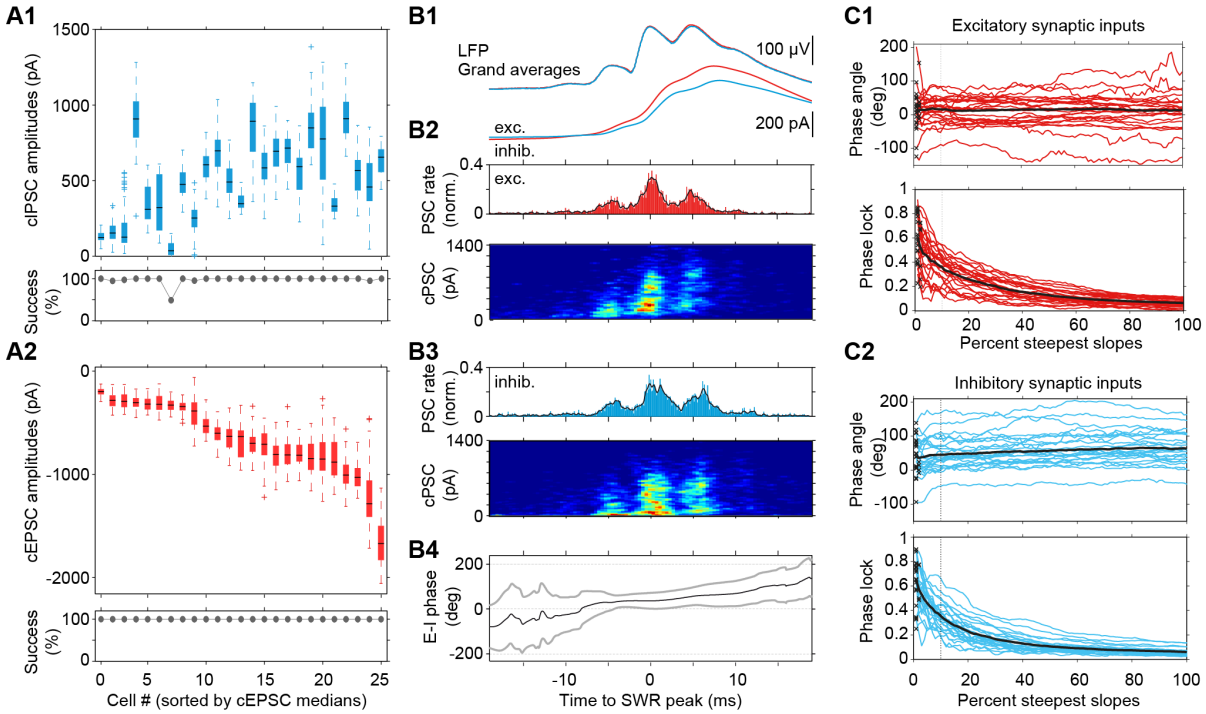

Figure S3. Amplitude and phase analysis of ripple-associated cPSC in MCs. Related to Figure 3.

A Peak current amplitudes of SWR-associated cIPSCs (recorded at +6 mV, **A1**, *top*) and cEPSCs (recorded at -60 mV, **A2**, *top*) were sorted by the medians of cEPSC amplitudes; *Bottom:* observation likelihoods (success rates) of cIPSCs and cEPSCs. We statistically compared the current trace surrounding the SWR peak (-20 ms to +45 ms) with a concatenated current trace containing data clearly separate from the given SWR event (-120 ms to -20 ms, and +45 ms to +120 ms with respect to the SWR peak; 175 ms duration in total). An unpaired two-sample, one-tailed *t* test, with α set to 0.1 was applied (right- and left-tailed testing for cEPSCs and cIPSCs, respectively). If the null hypothesis was rejected at $\alpha = 0.1$, the current sweep was classified as containing a synaptic event caused by the given SWR event, otherwise it was categorized uncoupled. For both, excitatory and inhibitory cPSCs, high success rate values were found. **B1** Grand averages, *upper* traces show LFPs, and *lower* the respective cPSCs, for excitatory (*red*, inverted) and inhibitory (*blue*) events. The ripple peak is the time reference in *B1-B4* (time point zero in *B4*). **B2 and B3** *Upper*: histograms (binsize = 0.1 ms, 400 bins) of the time points of the 10% strongest slopes of synaptic inputs, for excitatory (*B2*) and inhibitory (*B3*) PSCs. For all cells, the mean histogram over events was generated and normalized, corresponding to the empirical time-dependent input rate (number of inputs/ms). The resulting histograms were averaged and additionally smoothed with a Gaussian kernel (*black lines,* variance 0.2 ms). *Lower*: Amplitude-time histograms: Following the detection of the steepest slopes, the absolute amplitudes within the cPSCs were defined as the maximum values of the raw signal in the interval between the steepest increase (*i.e.*, the peak of the cPSC derivative) and the onset of the next synaptic input (*i.e.*, the following minimum of the cPSC derivative). The data were then binned in 2D histograms: The *x*-axis is the time difference of the steepest increase and the maximum peak of the LFP ripple signal as in the upper histogram (binsize 0.4 ms, 100 bins). The *y*-axis is the absolute amplitude (binsize 14 pA, 100 bins). The histogram was smoothed by convolution with a 2D Gaussian kernel (kernel width=1.5 bins; variance: 0.6 ms in *x*-axis and 21 pA in *y*-axis). To average over all cells, a histogram was generated for each cell with the sum over all bins normalized to 1, and then the average of all individual histograms was calculated. **B4** Temporal evolution of cEPSC-to-cIPSC phase difference. The excitatory and inhibitory traces were averaged and their Hilbert phases subtracted for each slice (*Grey lines*, SD). The cEPSC-to-cIPSC phase difference increased by 27.4° within the course of the LFP ripple (*i.e.* from -5 to +5 ms with respect to the ripple peak), corresponding to 0.53 ms on average (assuming 143 Hz median oscillation frequency in MC cEPSCs, as estimated by wavelet analysis; see main text). **C** Dependence of resulting phase and phase lock on the proportion of included events: a relative threshold was defined to decide whether a slope should be accepted as synaptic input or not, so that it would cover a fixed proportion of the possible extrema. To determine a reasonable value for this proportion, for all cells (**C1**, excitatory events; **C2**, inhibitory events), the average phase (*upper panel*) and phase lock (*lower panel*) were calculated for varying proportions (*x*-axis). Crosses denote the percentage for each cell that corresponds to 50 considered events; the *bold black lines* represent the averages over cells. *Dotted lines* correspond to the used proportion of events (10%). The average phase is robust with respect to changes in this percentage. The proportion of 10% was therefore chosen for the following two reasons: First, it is large enough to include a sufficient number of events (>50) for each cell; second, the phase lock at this percentage is high, indicating a low number of false-positive extrema.

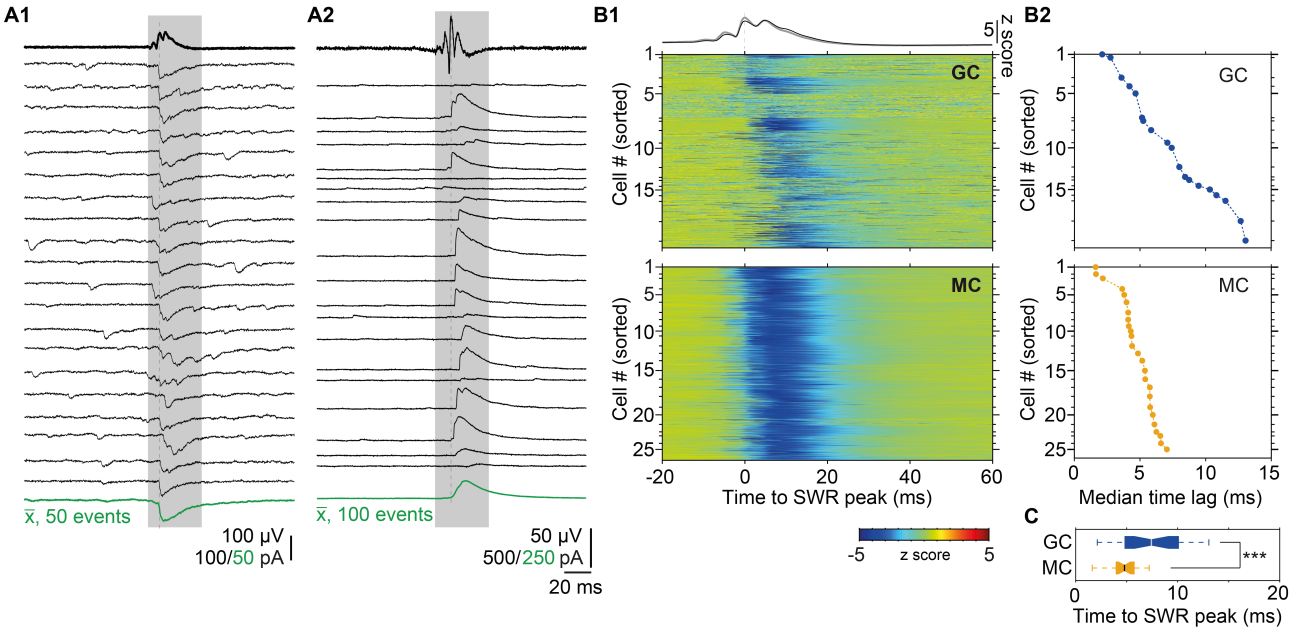

Figure S4. SWR-associated synaptic inputs in dentate gyrus GCs. Related to Figure 4.

A Examples displaying excitatory and inhibitory synaptic activity in GCs during CA3 SWRs in two independent recordings. Twenty successive sweeps of cEPSCs (V_{hold}, -60 mV, **A1**) and cIPSCs (V_{hold}, +6 mV, **A2**), centered on the peak of CA3 SWRs. *Green traces:* average of 50 and 100 sweeps for cEPSCs and cIPSCs, respectively. Synaptic inputs in GCs associated with SWRs are smaller on average than those observed in MCs. To separate spontaneous (not SWR-associated) and SWR-associated synaptic inputs, we used the following unbiased procedure to identify 'significant', *i.e.*, SWR-driven synaptic responses. We considered periods of 2 s centered on the maximum of the ripple peak (127-300 Hz filtered signal). Following baseline offset correction, the current sweeps were divided into 20 ms bins and the mean values were determined in each of the resulting 100 bins. With these values, a matrix of dimension 100× the number of SWR events in the given recording was created, where the row dimension corresponded to time and the column dimension corresponded to sweep numbers. Using repeated measures one-way ANOVA, all columns were pairwise compared. If the values in the SWR-related column were determined larger than those in the surrounding columns (determined with Tukey's *post-hoc* test at a level of $\alpha = 0.05$), the given cell was categorized as significantly modulated by SWR-related activity. Even in significantly modulated GCs, we found a high variability in amplitudes of both excitatory and inhibitory synaptic inputs (see examples in the main Figure 4). **B1** Color plots of individual SWR-modulated baseline-corrected cEPSC events in GCs (*above, n* = 19) and MCs (*below, n* = 25) displayed from -20 ms to 60 ms with respect to the SWR peak (*top:* z-scored grand averages of CA3 SWRs (black and grey) recorded simultaneously with GCs and MCs, respectively). The color bar (*bottom*) represents the z-scored amplitude values of cEPSCs. Cells were sorted according to their median time lag as shown in panel *B2*. The numbers of recorded cEPSCs varied between cells and hence the spacing between *y*-axis ticks is not equidistant. **B2** As for the analysis displayed in the main Figure 3E1, excitatory and inhibitory PSCs were low-pass filtered at 100 Hz (2^{nd} order Butterworth filter) and cross-correlated with the corresponding envelope of 100 Hz low-pass filtered SWRs (xcorr function in Matlab). The distribution of sorted cross-correlation derived median LFP-cEPSC time lags in GCs (*top*) and MCs (*bottom,* same as in the main Fig. 3E1) is displayed, corresponding to the colorplots shown in *B1*. **C** Comparison of median LFP-cEPSC time lags. SWR-cEPSC time lags are significantly prolonged in GCs compared to MCs ($P = 0.0008$, unpaired two-tailed *t* test).

Supplemental Experimental Procedures

Slice preparation. Following isoflurane-anesthesia, brains were transferred to ice-cold sucrose-based ACSF containing (in mM): 87 NaCl, 2.5 KCl, 3 $MgCl_2 \cdot 6H_2O$, 0.5 $CaCl_2$, 10 glucose, 50 sucrose, 1.25 NaH_2PO_4, and 26 $NaHCO_3$ (pH 7.4). Horizontal slices (400 µm) of ventral to mid-hippocampus were cut on a vibratome (VT1200S, Leica) and stored in an interface chamber perfused with ACSF containing (in mM): 119 NaCl, 2.5 KCl, 1.3 $MgCl_2$, 2.5 $CaCl_2$, 10 glucose, 1.25 NaH_2PO_4, and 26 $NaHCO_3$, at pH 7.4; osmolarity of 290 to 310 mosmol/l. The temperature was kept at ~32°C, and slices were superfused at a rate of ~1 ml/min. ACSF was equilibrated with carbogen (95% O_2, 5% CO_2). Slices recovered for >1.5 h after preparation.

Electrophysiology. Recordings were done in ACSF at 31-32°C in a submerged-type recording chamber perfused at 5-6 ml/min (Maier et al., 2009). For LFP recordings, glass microelectrodes (tip opening ~5-10 µm; 0.2-0.3 MΩ) were filled with ACSF. Whole-cell recordings were done with glass electrodes (2-5 MΩ) filled with either of two solutions containing (in mM): *(i)* 120 K-gluconate, 10 HEPES, 10 KCl, 5 EGTA, 2 $MgSO_4 \cdot 7H_2O$, 3 MgATP, 1 Na_2GTP, 14 phosphocreatine, and 5.4 biocytin (0.2 %); pH adjusted to 7.4 with KOH, or *(ii)* 117.5 gluconic acid, 8 NaCl, 10 TEA, 10 HEPES, 0.2 EGTA, 5 QX-314, 2.5 CsCl, 0.3 Na_2GTP, and 4 MgATP, 5.4 biocytin (0.2%); pH adjusted to 7.4 with CsOH. MC spiking was recorded for at least 10 min either in the cell-attached configuration (voltage clamp, VC, at -60 mV) using solution *(i)* or in on-cell recordings using ACSF-filled patch pipettes.

LFPs were amplified 1000× and whole-cell data were amplified 5× for VC and 10× for current-clamp recordings using a Multiclamp 700A or B amplifier (Molecular Devices). Data were low-pass filtered at 4 kHz (Bessel filter) and digitized at 20 kHz with 16-bit resolution using an A/D converter (BNC-2090 board, National Instruments, or Axon Digidata 1550A, Molecular Devices). Data were stored using Igor Pro (Wavemetrics) or pClamp (Molecular Devices). Series resistance (R_s) was monitored continuously; recordings were rejected if R_s exceeded 20 MΩ or varied >30%. No R_s compensation was used; no liquid junction potential correction was applied. For on-cell recordings, a candidate MC was chosen, and an ACSF-filled patch pipette placed on its soma. After recording of a sufficient amount of data, the pipette was removed and the cell re-approached with another pipette filled with intracellular solution and subsequently recorded in the whole-cell configuration, as described above.

Immunostainings and anatomical identification. Cells were routinely filled with 0.2% biocytin and slices were transferred to 4% paraformaldehyde for at least 3 h and maintained at 4° C in 0.1 M phosphate-buffered

saline (PBS) with 0.1% sodium-azide. For immunostainings, slices were washed 3× with 0.1 M PBS. The slices were blocked with 5% normal goat serum, followed by overnight incubation with streptavidin (1:500, Invitrogen) and mouse anti-GAD67 Ab (1:500, Millipore) at 4° C. Slices were then washed 3× in 0.1M PBS and incubated in Alexa 488 goat anti-mouse secondary Ab (1:500, Invitrogen), and Alexa 647 goat anti-mouse Ab (1:500, Invitrogen) for 2-4 h at room temperature. After washes in 0.1 M PBS, slices were mounted on slides and embedded in a mounting medium (Mowiol). Maximum intensity z-stack images were taken using a confocal microscope (Leica DMI 6000) with a 20× oil immersion objective. Reconstructions were done using the Simple Neurite tracer plugin in ImageJ (V 1.51).

Terminology. Hippocampal sharp waves (SPWs; Buzsáki, 1986) and ripples (O'Keefe and Nadel, 1978) were first characterized in behaving rats as fundamental signatures of normal EEG. However, the term *sharp wave* is also used in the context of clinical literature signifying a specific EEG graphoelement related to interictal epileptiform discharges (IED; Niedermeyer, 2005). Even though mechanistic properties, oscillation frequency, and information content carried by PC discharge during SWRs change in epilepsy (Aivar et al., 2014; Karlócai et al., 2014; Valero et al., 2017), physiological and epileptic sharp waves/ripples are likely to form a continuum of electrographic patterns expressed by the hippocampal network. Based on these studies, we follow a terminology where *sharp waves* (*SPWs*) and *ripples* (or *sharp wave-ripple complexes*, *SWRs*) refer to physiological activity patterns as opposed to IED and *fast ripples* or pathological ripples (*p-ripples*) (see also Traub and Whittington, 2010; Buzsáki, 2015).

References

Aivar, P., Valero, M., Bellistri, E., Menendez de la Prida, L. (2014). Extracellular calcium controls the expression of two different forms of ripple-like hippocampal oscillations. J Neurosci *34*, 2989–3004.

Buzsáki, G. (1986). Hippocampal sharp waves: Their origin and significance. Brain Res *398*, 242–252.

Buzsáki, G. (2015). Hippocampal sharp wave-ripple: A cognitive biomarker for episodic memory and planning. Hippocampus *25*, 1073–1188.

Karlócai, M.R., Kohus, Z., Káli, S., Ulbert, I., Szabó, G., Máté, Z., Freund, T.F., Gulyás, A.I. (2014). Physiological sharp wave-ripples and interictal events in vitro: What's the difference? Brain *137*, 463–485.

Maier, N., Morris, G., Johenning, F.W., Schmitz, D. (2009). An approach for reliably investigating hippocampal sharp wave-ripples in vitro. PLoS ONE *4*, e6925.

Niedermeyer, E. (2005). Abnormal EEG Patterns: Epileptic and Paroxysmal. In Electroencephalography Basic Principles, Clinical Applications, and Related Fields. Niedermeyer, E. and Lopes da Silva, F.H. ed. (Philadelphia, USA: Lippincott Williams & Wilkins), pp. 255–280.

O'Keefe, J. and Nadel, L. (1978). The hippocampus as a cognitive map. (Oxford: Oxford University Press).

Traub, R.D. and Whittington, M.A. (2010). Cortical Oscillations in Health and Disease (Oxford: Oxford University Press).

Valero, M., Averkin, R.G., Fernandez-Lamo, I., Aguilar, J., Lopez-Pigozzi, D., Brotons-Mas, J.R., Cid, E., Tamás, G., Menendez de la Prida, L. (2017). Mechanisms for selective single-cell reactivation during offline sharp-wave ripples and their distortion by fast ripples. Neuron *94*, 1234–1247.